Springer

KSME

Journal of Mechanical Science and Technology 33 (12) (2019) 5779~5786
www.springerlink.com/content/1738-494x(Print)/1976-3824(Online)
DOI 10.1007/s12206-019-1124-1

Effective vibration test planning method for equipment with high slenderness ratio †

Inki Park[1,2,*] and Junhong Park[2]

[1]*Agency for Defense Development, Daejeon 34186, Korea*
[2]*Department of Mechanical Engineering, Hanyang University, Seoul 04763, Korea*

(Manuscript Received July 20, 2019; Revised September 29, 2019; Accepted October 4, 2019)

Abstract

Vibration testing is necessary for functionality and durability evaluations of equipment that may undergo performance degradation due to operational vibrations. Here, we propose a planning method for the vibration testing of equipment with high slenderness ratios, such as missiles, and excitation, support, and measurement locations are important factors for the test configuration. A finite element model was used to calculate the normal modes and suitability indexes, based on the excitation and support locations. The measurement locations were obtained via the effective-independence method. Indexes of the response of dominant modes to excitation were generated for each surface through vibration testing involving various excitation, support, and measurement locations. The suitability indexes of excitation and support locations, exhibited a high correlation with the indexes of response magnitude in the dominant modes of the equipment. Therefore, the vibration test configuration can be planned effectively by exciting dominant modes of equipment under test.

Keywords: Excitation location; Measurement location; Performance degradation; Support location; Vibration test configuration

1. Introduction

Military equipment, such as missiles, are exposed to high levels of vibration during transportation and operation. Therefore, the reliability of these equipment need to be tested to ensure that the equipment is undamaged after they are exposed to excessive vibrations. Equipment exposed to excessive vibrations should be subjected to a vibration test during its development process. Numerous test standards have been proposed to guide vibration testing; these include the MIL-STD-810, DEF-STAN-00-35, and STANAG 4370 series. After launch, missiles are exposed to very high levels of external vibration during flight. This vibration is caused by engine exhaust, internal equipment operations, boundary layer turbulence, etc. [1]. This vibration input during missile flight has been expressed by wide-band random excitation [2]. The pressure spectrum of the boundary-layer turbulence has flat components in a frequency range up to 4 kHz. Hence, the vibration response of a missile is determined by its natural frequency responses to the random input [3]. To reproduce the vibration responses during missile flight in a laboratory, it is necessary to design and plan the vibration test configuration through complete examinations prior to testing. When determining the vibration responses during flight operations, the missile structure is not constrained, and the excitation force is applied on all surfaces of the airframe. These factors make it difficult to reproduce actual vibration response of missiles in a test laboratory. The reliability of the vibration test depends on the suitability of the design and planning of the configuration. For long and slender equipment such as air-carried missiles, there can be significant discrepancies in the measured service and test environments. This mismatch can largely be attributed to the test setup as fixture designs rarely replicate the in-service boundary conditions realistically, and the excitation path in the test can vary significantly from that in service [4].

The important factors that determine the configuration of the vibration test are the excitation, support, and measurement locations. The excitation location was determined to transmit the energy to vibrate the missile, and the exciter generates the force at specific locations on the missile surface. The supporting configuration of the missile was determined to allow a quasi-free boundary condition. The support locations were connected to the fixed structure of the test room by using bungee cords.

Imamovic studied the method of determining optimal locations for the test planning of aircraft-engine casings and nozzle vibrations [5]. The shortcoming of this method is that the stiffness distribution of the equipment is not considered. Therefore, the stiffness of the calculated excitation and support locations should also be considered to avoid exciting and supporting structurally weak locations.

This study proposes a systematic method to calculate the

*Corresponding author. Tel.: +82 2 2220 0424
E-mail address: pik@add.re.kr
† Recommended by Associate Editor Dongho Oh

Fig. 1. Shape of the aluminum-alloy missile model possessing high slenderness ratio.

optimal excitation, support, and measurement locations for vibration testing of equipment possessing high slenderness ratios, such as missiles. A finite-element model of the missile was created. The dominant modes influencing vibrational responses were selected from the results of the eigenmode analysis obtained by this finite element model. The suitability indexes were estimated to determine the excitation and support locations on the missile surface by using the eigenvector components of the dominant modes. The measurement locations were obtained using the effective-independence method that utilizes eigenvectors. Vibration tests of the actual missile model were conducted to verify the validity of the suitability indexes as the excitation, support, and measurement locations. The acceleration responses of the missile were measured for various setups of excitation, support, and measurement locations. Stability diagrams of the frequency-response function were obtained from the combinations of each setup. The response magnitudes of the dominant modes in each case were expressed via a simple index. Consequently, the suitability indexes obtained from the finite-element analysis were compared to the response-magnitude indexes of the dominant modes determined by the vibration tests. The response-magnitude index of the selected measurement locations and that of the comparative group were compared through the vibration test result. The results of the comparison of the indexes verified the effectiveness of the proposed test-planning method.

2. Vibration test configurations

2.1 Finite-element analysis of a missile structure

The missile structure used in this study is a hollow cylinder with a conical nose. The structure had a length of 1.4 m, outer diameter of 0.1 m, and thickness of 5 mm (rear half of the missile)/7 mm (front half of the missile). The structure is made of AL6061-T6 (Young's Modulus of 68.9 GPa, Poisson's ratio of 0.33, and density of 2700 kg/m^3) and has a total weight of 6.41 kg. The shape of the produced missile model is presented in Fig. 1.

The missile was modeled by the finite element model using MSC PATRAN and NASTRAN. Mode extraction was performed by using the Lanczos method. Through the normal

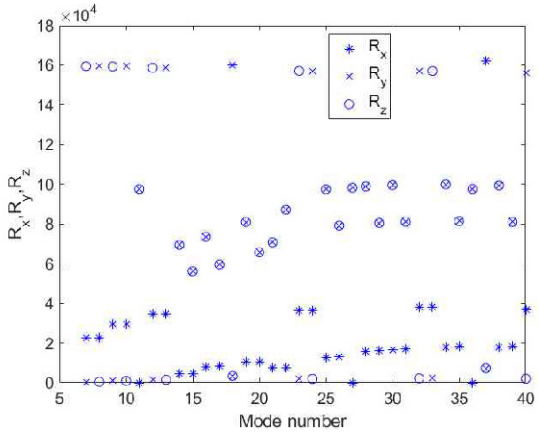

Fig. 2. Sum of the absolute values of eigenvectors in each orthogonal direction.

mode analysis, forty modes were extracted in order of increasing natural frequency, and the eigenvectors for each mode were calculated. The minimum and maximum values of the calculated natural frequencies were 307.9 Hz and 3950.3 Hz, respectively.

2.2 Dominant modes of vibration tests

When modal analysis is applied to a finite-element model, a number of normal modes equal to the number of degrees of freedom of all the elements are obtained mathematically. For efficient calculations, it is necessary to analyze the modes having a relatively large displacement with a significantly large contribution to the vibration responses. Determination of the dominant modes includes a visual inspection of the deformed shapes, in conjunction with modal effective mass and reaction evaluations, kinetic energy, group energy, element strain energy, and drive point residue methods [6]. An aeroservoelastic model of a slender anti-air missile was developed using discretizing continuous Euler-Bernoulli beams, which reduces the model to the first five bending modes that have a strong influence on vibration responses [7].

Generally, vibration tests for missiles are divided into three orthogonal (vertical, horizontal, and longitudinal) axes of the missile's body. Missiles are tested in the vertical and horizontal directions because the level of vibration in the longitudinal direction is smaller than that in the other directions [8]. The magnitudes of vibration in each orthogonal direction, for the lower frequency order of thirty-four modes, were compared based on the sum of the absolute values of eigenvectors as

$$R_{ij} = \sum \left| \phi_{ij} \right|_{(i=x,y,z)} . \tag{1}$$

The magnitudes of vibration in the vertical and horizontal directions were greater than those in the longitudinal direction, with the exception of two modes, as shown in Fig. 2.

The magnitudes of each mode were compared based on the

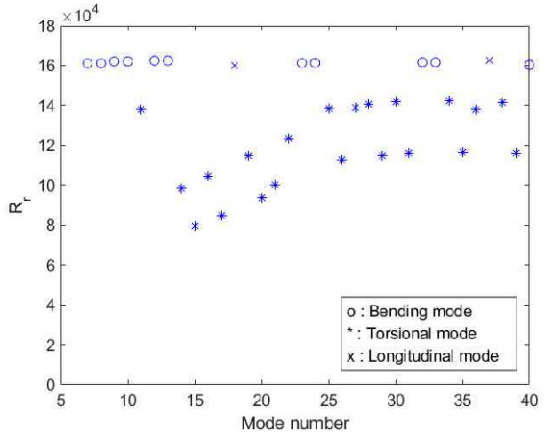

Fig. 3. Sum of the resultant response-vector magnitude for each mode.

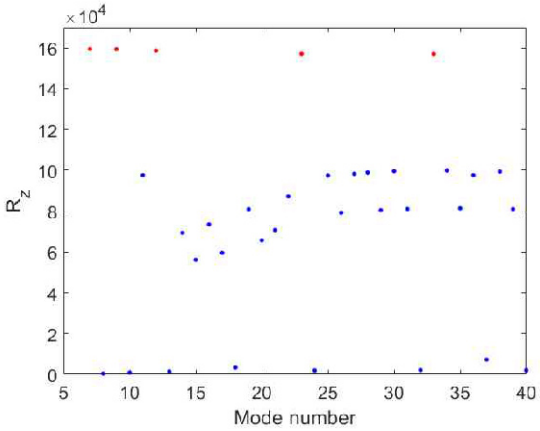

Fig. 4. Sum of the absolute values of all vertical-direction eigenvectors for each mode.

sum of the resultant vector magnitudes as

$$R_{rj} = \sum \left(\phi_{xj}^2 + \phi_{yj}^2 + \phi_{zj}^2 \right)^{0.5} . \quad (2)$$

The magnitudes of the torsional modes were less than those of the bending and longitudinal modes, as shown in Fig. 3. Therefore, torsional modes were not considered for the determination of dominant modes.

As the missile model used in this study was symmetrical in the vertical and horizontal directions, the vibration test was only considered in the vertical-direction. The dominant modes were selected according to the magnitude order of the sum of the absolute values of the vertical-direction eigenvector components of all the nodes in each mode shape [9]. The root-sum-square magnitude is expressed as

$$R_{zj} = \sum \left| \phi_{zj} \right| . \quad (3)$$

where R_{zj} is the sum of the absolute values of eigenvectors, and ϕ_{zj} are the eigenvectors of the j-th mode in the vertical direction. The modes with larger sums have higher overall motion and energy at specific locations. The calculated magnitude for the obtained normal modes is presented in Fig. 4.

As shown in Fig. 4, five modes were determined as the dominant modes with an order of magnitude R_{zj}. The modes selected by this method were 7, 9, 12, 23, and 33, and the natural frequency of each mode was 307.9, 810.1, 1478.2, 2251.1, and 3098.0 Hz, respectively. The mode shapes of the selected modes are shown in Fig. 5.

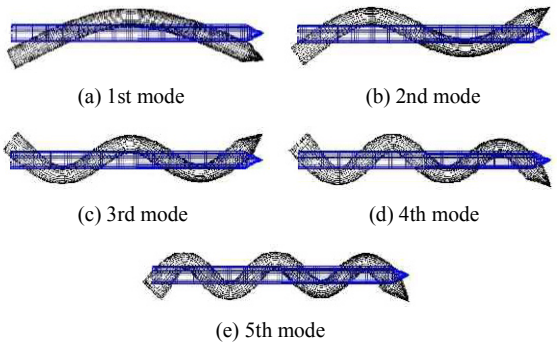

(a) 1st mode (b) 2nd mode

(c) 3rd mode (d) 4th mode

(e) 5th mode

Fig. 5. Mode shapes of the dominant modes' contribution to the vibration of the missile.

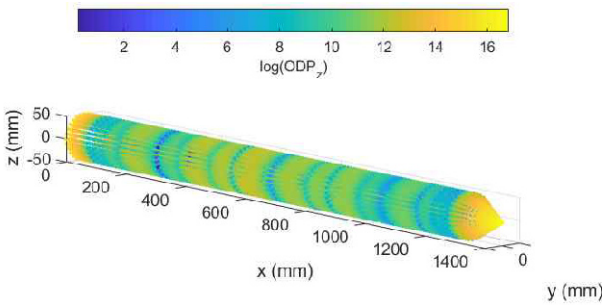

Fig. 6. ODP calculated to determine the excitation location.

2.3 Determination of excitation, support, and measurement locations

The locations of excitation, support, and measurement should be determined in advance to perform the vibration tests. In this study, the locations that cause the largest response in the dominant modes were obtained for the tests. The excitation location should not be close to the nodal points of any mode in order to induce a large response in the dominant modes. This is expressed by the suitability index for the excitation point, and defined as the optimal driving point (ODP) expressed as follows [10]:

$$ODP(i) = \prod_r \left| \phi_{i,r} \right| . \quad (4)$$

where r represents the mode number, and $\phi_{i,r}$ represents the eigenvectors of the mode. The ODP obtained by using the dominant modes is depicted in Fig. 6.

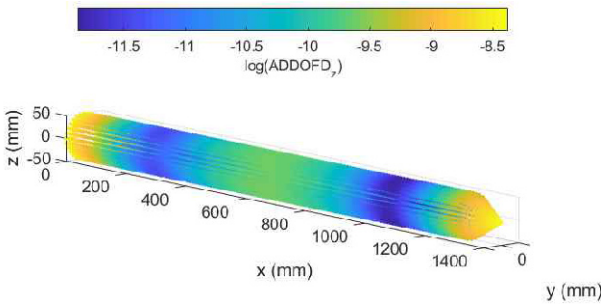

Fig. 7. ADDOFD calculated for determination of the support location.

The ODPs at both ends in the longitudinal direction were the largest. The dominant modes respond with the largest magnitude when the locations of large ODPs are excited. It is recommended in MIL-STD-810H that missiles should be excited at both ends during flight vibration tests [11].

The support location should minimize the interference between the binding force due to the test setup and the vibration motion of the missile. This is expressed by the suitability index as a support location. If it is assumed that the modes of the system are well spaced, the element of the receptance matrix evaluated at a natural frequency will be dominated by the term corresponding to that frequency [12]. The displacement amplitude of vibration is proportional to $\frac{\phi_{i,r}^2}{\omega_r^2}$, and the relationship is defined as the average driving point DOF displacement (ADDOFD), expressed as follows [13]:

$$ADDOFD(i) = \sum_r \frac{\phi_{i,r}^2}{\omega_r^2} . \quad (5)$$

where ω_r represents the natural frequency. The ADDOFD obtained by using the dominant modes is shown in Fig. 7.

As shown in Fig. 7, the ADDOFDs at the two locations are minimal. The dominant modes respond with a larger magnitude when supported at these locations. For missiles, the supporting force should be in equilibrium with the gravity.

During the vibration tests, only a limited number of vibration measurements can be used owing to various practical limitations. Therefore, it is desirable to select the minimum number of measurement locations to monitor the responses of the dominant modes. Optimal sensor placement was determined by the effective-independence method proposed by Kammer [14]. To measure the response of the missile, the response vector needs to be orthogonal to the contact surface of the accelerometer. The sensor locations should be on a straight line in the longitudinal direction on the surface, excluding the head of the missile. The minimum number of sensors to be instrumented should not be less than the number of mode shapes to be identified [15]. Accordingly, at least five measurement locations are required to identify the five mode shapes of the test object. By combining the eigenvectors of the five dominant modes, the prediction matrix was derived as follows.

$$[A]_{M\times M} = [\Phi]^T_{M\times N}[\Phi]^T_{N\times M} . \quad (6)$$

$$[E]_{N\times N} = [\Phi]_{N\times M}[A]^{-1}_{M\times M}[\Phi]^T_{M\times N} . \quad (7)$$

Removing one row in the N×M eigenvector matrix with the smallest value among the diagonal components of the N×N prediction matrix resulted in the (N-1)×M eigenvector matrix. The (N-1)×(N-1) prediction matrix was derived from the (N-1)×M eigenvector matrix, and the (N-2)×M eigenvector matrix was derived by removing one row in the (N-1)×M eigenvector matrix similarly. This process was repeated until the 5×5 eigenvector matrix was derived, and the locations corresponding to the rows where the 5×5 eigenvector matrix was initially placed in the N×M eigenvector matrix, were determined as the measurement locations. Consequently, the measurement locations were obtained as x = 10, 470, 660, 880, and 1290 mm, respectively.

3. Vibration tests for the missile

Vibration tests were performed with the missile model to verify the suitability indexes proposed in this study. For this purpose, an excitation force was applied by an electro-dynamic shaker, and acceleration responses of the missile were measured for various test configurations with different excitation, support, and measurement locations. A stability diagram of frequency-response function was generated from the measured input excitation force and acceleration responses. The response magnitude of the dominant modes in each test configuration was calculated.

The excitation locations for the vibration excitation-response test were determined at the local maximum and minimum locations of the ODP value in Fig. 6. The fifteen excitation locations were x = 10, 90, 220, 300, 430, 550, 600, 680, 750, 870, 920, 1050, 1120, 1250, and 1290 mm. The excitation force was delivered by connecting the armature head of the electro-dynamic shaker. The force sensor was attached with a stinger wire to decouple the dynamics of the missile from those of the shaker. Attaching the missile to the shaker table altered the dynamics significantly and resulted in unrealistic behavior [16]. The excitation force with a constant spectral shape of 10^{-5} kgf^2/Hz at a frequency range of 100–3500 Hz was applied as a reference force profile. The force measured from the piezoelectric force sensor was fed back to a vibration controller to follow this reference profile in real time. When the two locations were excited by the same force profile simultaneously, the excitation spectra were uncorrelated. When the configuration of the tested structure has a high slenderness ratio, the multi exciter test (MET) provides a distribution of vibration energy more effectively than the single exciter test (SET), which is a significant advantage for reliability tests [17].

The support locations for the vibration excitation-response

Fig. 8. Vibration test configuration of the missile involving two electro-dynamic shakers and two bungee cords.

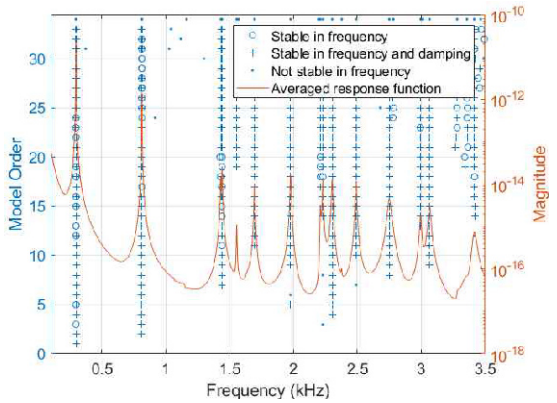

Fig. 9. Averaged FRF and stabilization diagram.

test were determined at two local minimum locations, namely x = 280 and 1070 mm in Fig. 5, and at the ten locations of x = 30, 150, 440, 510, 580, 860, 930, 1000, 1150, and 1270 mm for comparison. The missile was supported by elastic bungee cords at the bottom and then suspended from the upper fixed structure to simulate the free-free boundary conditions.

The measurement locations were determined as x = 10, 470, 660, 880, and 1290 mm from the effective independence method, and at the six locations of x = 150, 300, 550, 750, 1000, and 1150 mm for comparison. The mounting bases were attached to the missile by using adhesives, and the accelerometers were attached. Acceleration and force were acquired at a sampling rate of 10 kHz. The vibration test configuration of the missile is illustrated in Fig. 8.

From the vibration tests, stabilization diagrams were calculated with MATLAB by using the averaged input force and output acceleration response. The least-squares rational-function method [18] was used for the single input excitation, and the least-squares complex-exponential method [19] was used for the two input excitations. A stabilization diagram is used to fit models with higher orders to identify the true structural modes [20]. The rate of change of frequency and damping ratio converged to less than 1 % and 5 %, respectively. The stabilization diagram obtained for the case of excitation at x = 10 mm, support at x = 280 and 1070 mm, and measurement at all eleven locations is shown in Fig. 9.

Table 1. Natural frequencies for the dominant modes.

Mode no.	Frequency (Hz) (FEM)	Frequency (Hz) (Test)	Frequency difference (%)	FRF magnitude (10^{-14} m/(s^2·N)) (Test)
1	308	298	3.5	18000
2	810	813	0.3	1400
3	1478	1432	3.3	14
4	2251	2210	1.9	3.1
5	3098	2995	3.5	1.8

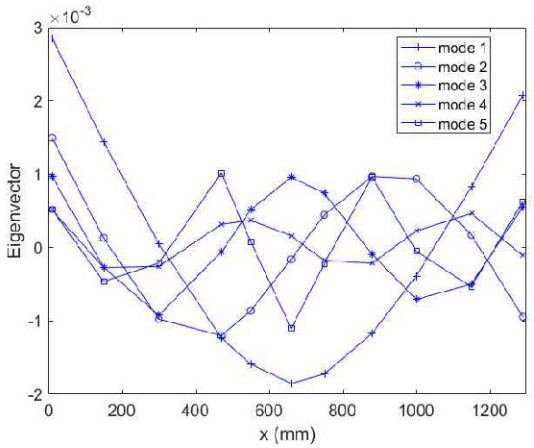

Fig. 10. Mode shapes for the dominant modes.

The natural frequencies corresponding to the dominant modes were verified by the mode shapes plotted in Fig. 10. The measured mode shapes correlate well with the predicted mode shapes in Fig. 5. The natural frequencies for each target mode obtained from the FEM analysis and those obtained from the vibration test are compared in Table 1.

The following function is defined to represent the response magnitudes of the modes of interest as a single index.

$$O_F(xi) = \prod \left| \frac{A(\omega)}{F(\omega)} \right|_{(m,xi)} . \tag{8}$$

where O_F is the multiplications of magnitudes of the FRF at the natural frequency of the mode of interest when the location xi was excited. By multiplying the magnitudes of the FRF, it is possible to consider the magnitudes of each FRF equally, despite large differences in the levels of FRF magnitudes for each mode. A higher response magnitude indicates a more appropriate excitation location similar to the ODP value. The response magnitude obtained from the vibration test and the ODP values in Fig. 6. are compared in Fig. 11.

In Fig. 11, '*' denotes a case with excitation at one location and 'o' denotes a case with dual excitations. The magnitude of the measured and predicted responses exhibits similar variations. The response magnitude of the dual excitations is larger than that of the single excitation. The response of the dominant modes increased when they were excited at locations

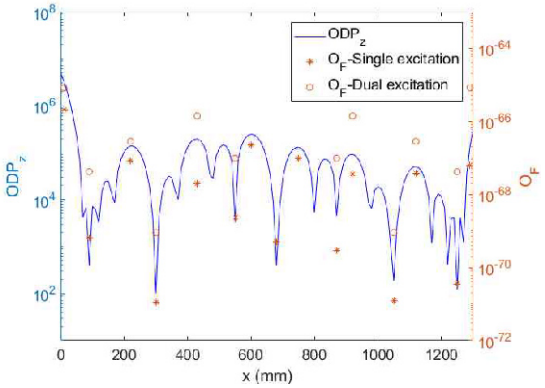

Fig. 11. ODP from FEM analysis and O_F from vibration tests.

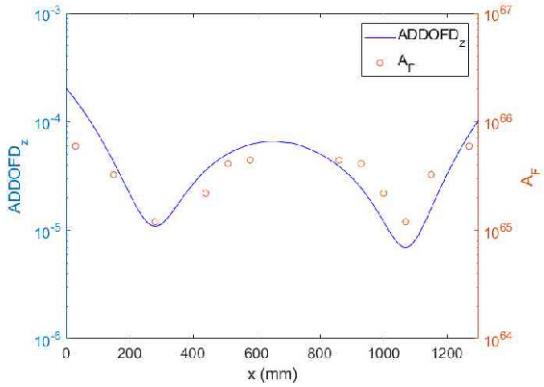

Fig. 13. ADDOFD from FEM analysis and A_F from vibration tests.

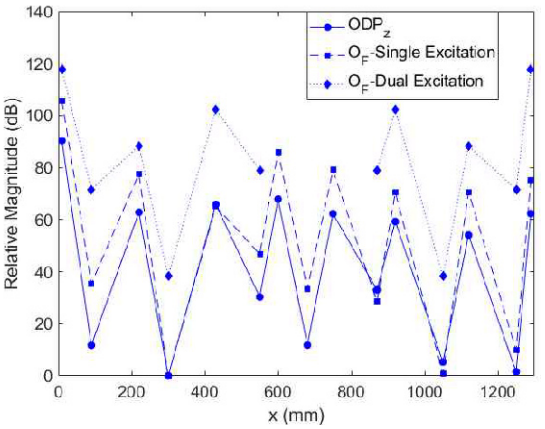

Fig. 12. Comparison of relative magnitudes from FEM analysis (ODP) and from vibration tests (O_F).

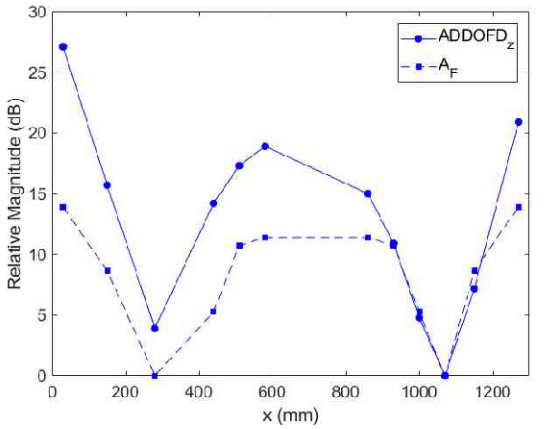

Fig. 14. Comparison of relative magnitudes from FEM analysis (ADDOFD) and from vibration tests (A_F).

inducing large vibration responses. The indexes in Fig. 11 were defined to indicate the relative effectiveness of inducing vibration due to the variation in the excitation location. The relative magnitudes referenced to their individual minimum values at each excitation location are also expressed by a decibel unit to clarify the comparison, as shown in Fig. 12.

Fig. 12 presents the relative variation of the sensitivity with respect to the excitation locations. The overall measured responses of the dominant modes (O_F) increased when the locations with large predicted sensitivities (ODP) were excited. The optimal excitation locations calculated by the sensitivity were validated by the multiplication of the FRF magnitudes proposed in this study.

The following function was defined to represent the response magnitude of the modes of interest as a single index.

$$A_F(xi) = \prod \left| \frac{A(\omega)}{F(\omega)} \right|^{-1}_{(m,xi)} . \tag{9}$$

where $A_F(x_i)$ is the product of all the inverse numbers of the FRF magnitude at the natural frequency of the mode of interest m when location xi is supported. The lower value of A_F indicates a more appropriate support location similar to the ADDOFD value. The A_F values obtained from the vibration test and the ADDOFD values presented in Fig. 7 are compared, as shown in Fig. 13.

In Fig. 13, the measured and predicted indexes exhibit the same tendency. The response of the dominant modes increased when the location of a smaller ADDOFD was supported. The indexes in Fig. 13. were defined to show the relative effectiveness as a support location. The relative magnitudes of indexes referenced to their individual minimum values are represented by a decibel unit in Fig. 14 to clarify the comparison.

The overall response of the dominant modes that are the inverse of A_F increased when locations with smaller ADDOFD were supported. The optimal support locations calculated by the ADDOFD method were validated by the index of FRF magnitude multiplications proposed in this study.

The following function is defined to represent the response magnitude of the interested modes for a combination of measurement locations as a single index.

$$E_F(i_{set}) = \prod \left| \frac{A(\omega)}{F(\omega)} \right|_{(m,i_{set})} . \tag{10}$$

Table 2. FRF magnitude product for each measurement location.

Measurement set No.	Measurement locations (mm)	E_F (10^{-70} (m/(s^2·N))^5)		
		Excitation at 10 mm	Excitation at 1290 mm	Excitation at 10 mm and 1290 mm
1	10, 470, 660, 880, 1290	2292	41.0	4256
2	150, 300, 550, 750, 1000	83	3.7	459
3	150, 300, 550, 750, 1150	84	2.9	419
4	150, 300, 550, 1000, 1150	53	1.9	330
5	150, 300, 750, 1000, 1150	55	2.0	456
6	150, 550, 750, 1000, 1150	62	2.2	375
7	300, 550, 750, 1000, 1150	82	3.0	467

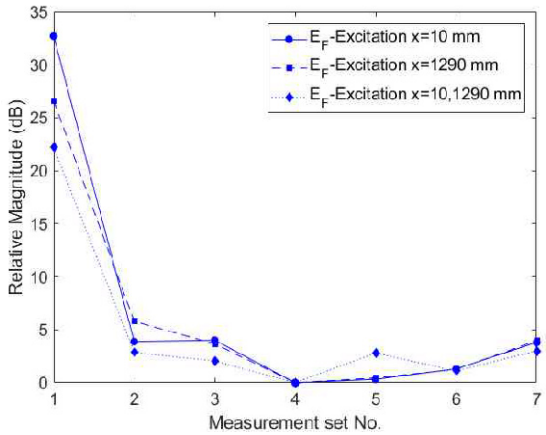

Fig. 15. Relative magnitudes comparison of E_F from vibration tests.

The E_F values obtained from the combination of measurement locations are compared as shown in Table 2.

In Table 2, the FRF magnitude multiplication is the largest when the response was measured at locations determined by the effective-independence method. The results are equal for the three different cases of excitation locations. The support locations were kept constant at x = 280 and 1070 mm. The response of the dominant modes was observed to be largest when measured at locations determined by the effective-independence method, regardless of the excitation location. The response sensitivity (E_F) was defined to indicate the relative effectiveness at a measurement location. The relative magnitudes of E_F at each measurement location set referenced to their individual minimum values from different excitation cases are shown by a decibel unit in Fig. 15 for a clearer comparison.

The maximum relative magnitudes were obtained in measurement set 1 and were compared to those of the other combinations. Measurement set 1 was determined by inducing the minimum number of sensor locations needed to observe the dominant modes as independently as possible. The remaining sets were selected using evenly distributed locations different from those of set 1 for comparison. The optimal measurement locations calculated by the effective-independence method were validated by the measured FRF-magnitude multiplications.

4. Conclusions

In this study, an effective method to determine the locations of excitation, support, and measurement for the planning of vibration tests for equipment possessing high slenderness ratios, such as missiles, was investigated. The suitability indexes for each location of the excitation and support calculated from the finite-element model, and the response indexes of the dominant modes from vibration tests exhibited similar trends. The effectiveness of the method to determine excitation and support locations was verified by the results of the tests. The highest vibration response was measured at the locations determined by the effective-independence method. The effectiveness of the method in determining the measurement locations was verified by tests. This method to determine the locations of excitation, support, and measurement was effectively applied for the missile model. However, when this method is used, the availability of excitation, support, and measurement locations should also be investigated by considering the structural constraints of the equipment. It is necessary to verify the scalability of the proposed method by using actual equipment with more complex shapes and compositions. The results of this study provide a systematic method to determine the fundamental test configuration elements that are required when planning vibration tests, especially for equipment possessing high slenderness ratios.

Acknowledgments

This research was supported by the Infrastructure Building Program through the Korea Agency for Infrastructure Technology Advancement (KAIA), which is funded by the Ministry of Land, Infrastructure and Transport (19CTAP-C153014-01-000000).

References

[1] *MIL-STD-810H (Environmental Engineering Considerations and Laboratory Tests)*, 514.8D-14, Department of Defense, USA (2019).

[2] *DEF STAN 00-35 (Environmental Handbook for Defense Materiel)*, Part5 Issue4 Chapter7-01, Ministry of Defence, UK (2006) 124-125.

[3] *MIL-STD-810H (Environmental Engineering Considerations and Laboratory Tests)*, 523.4-4, Department of Defense, USA (2019).

[4] C. Roberts and D. Ewins, Multi-axis vibration testing of an aero dynamically excited structure, *Journal of Vibration and Control,* 24 (2) (2016) 428.

[5] N. Imamovic, Validation of large structural dynamics models using modal test data, *Doctorial Thesis*, Imperial College of Science, Technology and Medicine, University of London

(1998).
[6] H. Hidalgo Jr., An innovative structural mode selection methodology: Application for the X-33 launch vehicle finite element model, *AIAA-2000-1587* (2000) 1.
[7] A. Verhaegen and R. Zbikowski, Aeroservoelastic modelling and control of a slender anti-air missile for active damping of longitudinal bending vibrations, *Aerospace Science and Technology,* 66 (2017) 9.
[8] *MIL-STD-810H (Environmental Engineering Considerations and Laboratory Tests)*, 514.8-20, Department of Defense, USA (2019).
[9] H. Hidalgo Jr., An innovative structural mode selection methodology: Application for the X-33 launch vehicle finite element model, *AIAA-2000-1587* (2000) 2.
[10] D. J. Ewins, *Modal Testing-theory, Practice and Application*, Research Studies Press, UK (2000) 510.
[11] *MIL-STD-810H (Environmental Engineering Considerations and Laboratory Tests)*, 514.8-20, Department of Defense, USA (2019).
[12] D. J. Inman, *Engineering Vibration*, Pearson, UK (2014) 610.
[13] D. J. Ewins, *Modal Testing-theory, Practice and Application*, Research Studies Press, UK (2000) 509.
[14] D. C. Kammer, Sensor placement for on-orbit modal identification and correlation of large space structures, *Journal of Guidance, Control and Dynamics,* 14 (2) (1991) 251-259.
[15] T. Yi and H. Li, Methodology developments in sensor placement for health monitoring of civil infrastructures, *International Journal of Distributed Sensor Networks* (2012) 8.
[16] P. M. Daborn, P. R. Ind and D. J. Ewins, Enhanced ground-based vibration testing for aerodynamic environments, *Mechanical Systems and Signal Processing,* 49 (2014) 166.
[17] *MIL-STD-810H (Environmental Engineering Considerations and Laboratory Tests)*, 527.2-2, Department of Defense, USA (2019).
[18] H. Vold, J. Crowley and G. T. Rocklin, New ways of estimating frequency response functions, *Sound and Vibration,* 18 (1984) 34-38.
[19] D. L. Brown, R. J. Allemang, R. Zimmerman and M. Mergeay, Parameter estimation techniques for modal analysis, *SAE Transactions,* 88 (1) (1979) 828-846.
[20] P. Avitabile, *Modal Testing-a Practitioner's Guide*, Wiley, New Jersey, USA (2018) 208.

Inki Park received a B.S. degree from Korea Aviation University in 1997 and an M.S. degree from Hanyang University in 2002. He is currently a researcher at the Agency for Defense Development, and a Ph.D. candidate at the Graduate School of Hanyang University. His research interest is the environmental vibration test method for a large EUT.

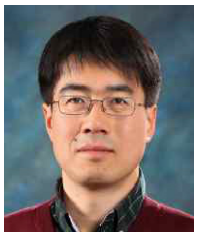

Junhong Park received B.S. and M.S. degrees from the Korea Advanced Institute of Science and Technology (KAIST) in 1991 and 1993, respectively. He received a Ph.D. degree from Purdue University in 2002. He is currently a Professor of Mechanical Engineering at Hanyang University. His research interests are signal processing, wave analysis, and noise control for improving the acoustic comfort of automobiles, trains, and residential buildings.